

Homodyne Detection Quadrature Phase Shift Keying Continuous-Variable Quantum Key Distribution with High Excess Noise

Wen-Bo Liu,¹ Chen-Long Li,¹ Yuan-Mei Xie,¹ Chen-Xun Weng,¹ Jie Gu,¹ Xiao-Yu Cao,¹ Yu-Shuo Lu,¹ Bing-Hong Li,¹ Hua-Lei Yin,^{1,*} and Zeng-Bing Chen^{1,†}

¹*National Laboratory of Solid State Microstructures,
School of Physics and Collaborative Innovation Center of Advanced
Microstructures, Nanjing University, Nanjing 210093, China*

Discrete-modulated continuous-variable quantum key distribution with homodyne detection is widely known for the simple implementation, efficient error correcting codes and the compatibility with modern optical communication devices, in which the quaternary modulation offers remarkable performance so far. However, quaternary modulation reduces the tolerance of excess noise and leads to insufficient transmission distance, thus seriously restricting the large-scale deployment of quantum secure communication networks. Here, we propose a new homodyne detection protocol using the technology of quadrature phase shift keying. By cutting down information leakage, our protocol pulls excess noise tolerance back to a high level. Furthermore, we demonstrate that the superiority of heterodyne detection in excess noise tolerance is due to the less information leakage rather than the ability of measuring both quadratures simultaneously. The security is analyzed by tight numerical method against collective attacks in the asymptotic regime. Results show the improvement of excess noise tolerance, which implies the ability to distribute keys in near intercity area. This progress will make our protocol the main force in constructing low-cost quantum secure communication networks.

I. INTRODUCTION

A growing body of achievements in quantum computing [1, 2] recently implies a new era is close at hand, which threatens modern secure communications. For instance, the most widely used public key system, Rivest-Shamir-Adleman cryptosystem [3], whose security relies on the complexity of factoring large number, can be illegally cracked by factoring algorithm [4] with quantum computer. Therefore, an encryption algorithm which can offer security against quantum attacks is urgently needed. One-time pad algorithm [5] is the one which promises the information-theoretically secure communication if two remote users share identical secret keys and use each bit of keys only once during encrypting. Although the promise is tempting, sharing sufficient keys is a tough task for modern cryptography. Quantum key distribution (QKD) [6–10] can distribute identical secret keys against the general attacks.

The main difficulty of realizing QKD is usually due to the mismatch between theoretical requirements and experimental conditions. Discrete-variable quantum key distribution (DV-QKD), especially the one proposed by Bennett and Brassard in 1984 [6], has developed rapidly since it was presented. So far, there are plenty of protocols based on various discrete degrees of freedom of single photon such as polarization [11–13] and time-bin [14, 15]. The security of most protocols has been generalized to resist coherent attacks in finite-key condition [16]. Many attempts have been made to realize network deployment

of DV-QKD [17]. However, detecting single photon and generating keys require sophisticated and strict experiment technology and devices. Compared with DV-QKD, in the aspect of experiment, continuous-variable quantum key distribution (CV-QKD) [8, 18] has more outstanding performance. Encoding keys in quadratures of the quantized electromagnetic field, CV-QKD is naturally compatible with classical coherent optical communication facility. Nevertheless, the simplicity of the experiment conversely puts forward a high demand for the security analysis.

With different security analysis, there are two main modulation methods of CV-QKD: Gaussian-modulation and discrete-modulation. Since both quadratures obey the Gaussian distribution with required variance, Gaussian-modulated protocols [19–22] possess U(n) symmetry and have a relatively complete security analysis [23–27]. However, new efficient error correction methods are needed for continuous-to-discrete mapping. Moreover, modulation continuity of both quadratures would never be satisfied in the experiment [28–31], leading to an irreparable loophole in security. Discrete-modulated protocols [32–36] have great advantages over Gaussian-modulated protocols in experiment. The preparation is largely simplified since only few kinds of signals different in phases are required. The general error correction method for discrete variables is still applicable. And the security deals with the discontinuity of modulation, thus the loophole of continuity is leaped over naturally. Brilliant numerical methods for security analysis are constantly emerging [37–39] and analysis methods follow up [40], even though the discrete modulation lacks U(n) symmetry. Finally, the security against collective attacks in the asymptotic regime has been proved. Further improvement of security can be expected soon.

* hlyin@nju.edu.cn

† zbchen@nju.edu.cn

The price for discrete-modulated CV-QKD to own these advantages is shorter transmission distance and sub-optimal secret key rates. The protocols including homodyne detection perform poorly in excess noise tolerance theoretically [38]. No matter how robust and close to the ideal device the homodyne detector is in experiment, this drawback would cause experimental advantages useless. In review of Gaussian-modulated protocols, homodyne detection is the most adopted detection method [41–47] in experiment, outperforming the heterodyne detection that enables to measure both quadratures simultaneously [48, 49]. However, in discrete modulation, the protocols including heterodyne detection seems to offer much longer transmission distances, which makes it more favored by theoretical researchers. It is natural to raise a question: why heterodyne detection protocols have a great advantage over homodyne detection protocols in secret key rates and transmission distances when applying discrete modulation. It seems that the promotion is attributed to the measurement operator [50–52]. We will show that homodyne detection also has chance to transmit secret key in long distance.

In this work, we offer a new quaternary-modulated protocol with homodyne detection. Different from previous protocols [37, 38] with quaternary modulation, we rotate the phase of the signals by $\frac{\pi}{4}$, which fits the classical quadrature phase shift keying (QPSK) method well in implementation. Due to homodyne detection, Bob still measures one of quadratures each round, but Alice generates her raw key according to Bob's choice. By this interesting operation, our protocol shows good tolerance of excess noise and promises significantly longer transmission distances than previous homodyne detection protocol [38].

We introduce our protocol in Section II, with an instruction of a possible experimental setup. In Section III, the formula of secret key rate is given against collective attacks in the asymptotic regime. In Section IV, we numerically simulate the performance of our protocol, which demonstrates the promotion in transmission distances. The interpretation of this phenomenon and some further discussions are shown in Section V.

II. PROTOCOL DESCRIPTION

The scheme of our protocol is illustrated in this section, with preparing and mapping method in Fig. 1 and experimental diagram in Fig. 2.

(1) *State preparation.*— For each round, Alice prepares one of four coherent states in set $\{|\alpha e^{i\frac{\pi}{4}}\rangle, |\alpha e^{i\frac{3\pi}{4}}\rangle, |\alpha e^{i\frac{5\pi}{4}}\rangle, |\alpha e^{i\frac{7\pi}{4}}\rangle\}$ with equal probability. These states are only different in phases. She sends the prepared state to Bob.

(2) *Measurement and mapping.*— After receiving Alice's state from quantum channel, Bob selects a quadrature from $\{\hat{q}, \hat{p}\}$ with the same probability. He performs

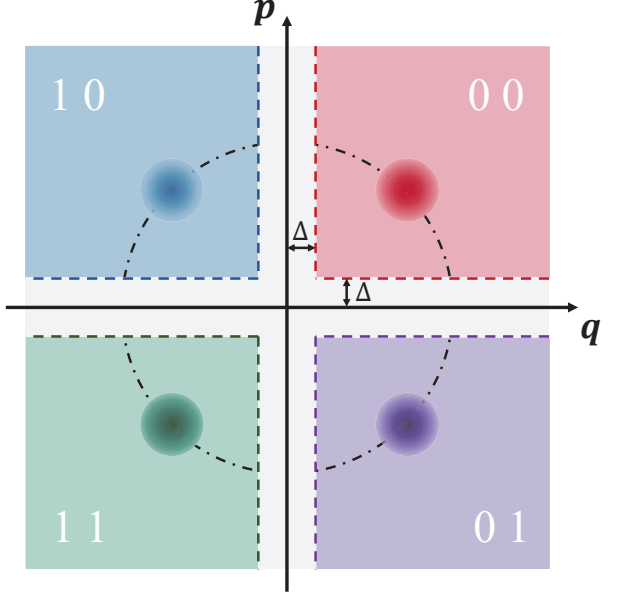


FIG. 1. Quaternary phase shift keying and key mapping of our protocol. Sender Alice randomly sends one coherent state with amplitude α and phase $\theta \in \{\frac{\pi}{4}, \frac{3\pi}{4}, \frac{5\pi}{4}, \frac{7\pi}{4}\}$ each round, representing labels $\{00, 10, 11, 01\}$ respectively. Receiver Bob randomly measures one quadrature from $\{\hat{q}, \hat{p}\}$ each round, and gets the outcome q or p respectively. He maps the outcome greater than Δ into bit 0 and the outcome smaller than $-\Delta$ into bit 1 for both quadratures. After announcement, Alice records the first bit of label if state is measured in \hat{q} or the second bit of label if state is measured in \hat{p} as her key bit.

corresponding homodyne detection of chosen quadrature on the state and obtains the measurement outcome.

(3) *Announcement and parameter estimation.*— After sufficient rounds of the above two steps, Alice and Bob communicate through an authenticated public channel. Bob announces his choice of quadratures. All rounds are separated into two groups according to quadratures. Alice and Bob randomly select a test subset from each group. Then they disclose the sending state and outcomes of each round in test subset. According to the information they exposed, they calculate the secret key rate under reverse reconciliation. If the calculations show no secret key can be generated, they abort the protocol. Otherwise, they proceed.

(4) *Raw key generation.*— Alice and Bob can obtain their raw keys using the remaining rounds. Suppose there are M rounds left, they can be numbered by the order of sending. For k th round, Alice labels the corresponding state $|\phi_k\rangle \in \{|\alpha e^{i\frac{\pi}{4}}\rangle, |\alpha e^{i\frac{3\pi}{4}}\rangle, |\alpha e^{i\frac{5\pi}{4}}\rangle, |\alpha e^{i\frac{7\pi}{4}}\rangle\}$ as $a_k \in \{00, 10, 11, 01\}$ respectively. Then the key bit x_k is equal to the first bit of label a_k when the round is measured in \hat{q} , and equal to the second bit of a_k when

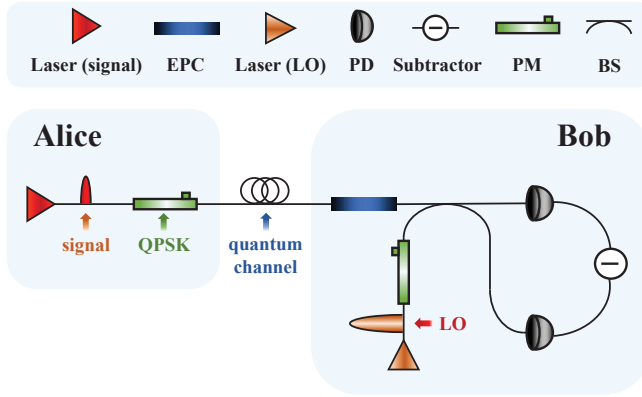


FIG. 2. Experimental schematic of our protocol. To avoid Eve manipulating local oscillator (LO) transmitted from Alice, we adopt the local LO scheme. Abbreviations and functions of components in the figure: EPC, electrical polarization controller, is used to control the polarization of signal light from Alice; PD, photodetector, is used for the detection of light; PM, phase modulator, is used for modulating the phase of light; QPSK, quadrature phase shift keying, is a technology modulating phase into $\{\frac{\pi}{4}, \frac{3\pi}{4}, \frac{5\pi}{4} \text{ or } \frac{7\pi}{4}\}$; BS, beam splitter, is used for interfering signal light and LO.

the round is measured in \hat{p} . Thus she obtains her string $\mathbf{X}' = (x_1, \dots, x_k, \dots, x_M)$. Bob maps the outcome q_k of \hat{q} or the outcome p_k of \hat{p} greater than Δ into bit 0 and the outcome smaller than $-\Delta$ into bit 1. Outcomes with other values are mapped into \perp . The image of mapping is exactly the raw key z_k . Finally, he obtains his string $\mathbf{Z}' = (z_1, \dots, z_k, \dots, z_M)$. Δ is a non-negative parameter and related to postselection. A protocol without postselection can set $\Delta = 0$. Alice and Bob communicate with each other and delete positions with symbol \perp from their strings. In the end, they obtain their raw key strings \mathbf{X} and \mathbf{Z} .

(5) *Error correction and privacy amplification.*— Alice and Bob choose suitable methods to conduct error correction and privacy amplification. Finally they generate secret keys.

A realistic experiment setup of our protocol with local oscillator (LLO) is proposed in Fig. 2. Necessary components are displayed in the figure with some unnecessary details omitted. Our schematic includes two parts, namely Alice and Bob.

In each round, Alice first prepares one of four signal states using a phase modulator implementing QPSK. Afterwards, the signal light is transmitted through a quantum channel and Bob receives the light. The polarization of signal light is corrected by electrical polarization controller (EPC). Bob generates LLO with phase randomly chosen from $\{0, \frac{\pi}{2}\}$ using phase modulator. In the end, the signal light and LLO are sent into beam splitter and interfered. The photodetector jointed by a subtractor reveals the result of the outcome. After getting outcomes, Alice and Bob conduct post-processing described by steps (3)-(5) on their data and we do not show this part in the

figure.

III. THE SECRET KEY RATE

We should evaluate the secret key rate before generating secret key. The entanglement-based protocol is considered, then we can write the key rate formula of our protocol.

A. Entanglement-based protocol

An equivalent entanglement-based protocol of our protocol can be described below. Alice prepares an entangled state

$$|\Phi\rangle_{AA'} = \sum_x \sqrt{p_x} |x\rangle_A |\phi_x\rangle_{A'}, \quad (1)$$

where the subscripts A and A' represent two entangled systems. x represents one of four labels in $\{00, 10, 11, 01\}$. $p_x = 0.25$ means equivalent probability to collapse into label x . Four states $\{|x\rangle\}$ are the orthogonal bases of system A , which can be measured by a set of POVM $\{M^x = |x\rangle\langle x|\}$. Four states $\{|\phi_x\rangle\}$ are $\{|\alpha e^{i\frac{\pi}{4}}\rangle, |\alpha e^{i\frac{3\pi}{4}}\rangle, |\alpha e^{i\frac{5\pi}{4}}\rangle, |\alpha e^{i\frac{7\pi}{4}}\rangle\}$ respectively. A is kept by Alice and A' is sent to Bob via a quantum channel. Thus the final state is given by

$$\rho_{AB} = (\mathbb{I}_A \otimes \mathcal{E}_{A' \rightarrow B})(|\Phi\rangle_{AA'} \langle \Phi|), \quad (2)$$

where $\mathcal{E}_{A' \rightarrow B}$ is a completely positive and trace-preserving (CPTP) mapping. This mapping includes the influence of the environment and the attacks of Eve. Alice randomly projects the system A into an eigenstate by $\{M^x\}$ then she can write down the label x without additional operation. Bob measures the system B as with the step (2) in our prepare-and-measure protocol and follows left steps.

B. Key rate formula

When applying reverse reconciliation, it means that Alice corrects her bits according to Bob's string, which implies that adversary Eve should try her best to guess Bob's string. For the case that Eve performs collective attacks in the asymptotic regime, the secret key rate formula [38, 53] is given by

$$R^\infty = p_{\text{pass}} \min_{\rho_{AB} \in \mathbf{S}} H(\mathbf{Z}|E) - p_{\text{pass}} \delta_{EC}, \quad (3)$$

in which p_{pass} is the probability of preserving a round to generate key. The conditional von Neumann entropy $H(\mathbf{Z}|E)$ describes the uncertainty of string \mathbf{Z} in Eve's view. Eve's maximal knowledge of Bob's string \mathbf{Z} leads to the minimal uncertainty of \mathbf{Z} under a certain density

matrix ρ_{AB} . To evaluate Eve's maximal knowledge when ρ_{AB} is uncertain for Alice and Bob, we need to find the minimal conditional entropy $H(\mathbf{Z}|E)$ of all ρ_{AB} that conforms to the constraints \mathbf{S} . $\delta_{EC} = H(\mathbf{Z}) - I(\mathbf{X}; \mathbf{Z})$ is the amount of information leakage in each round. $H(\mathbf{Z})$ is related to the probability distribution of Bob's measurement outcomes. $I(\mathbf{X}; \mathbf{Z})$ represents the classical mutual information between two strings.

Since Bob announces the measurement quadrature of each round, they can analyze the security of each quadrature separately. We can rewrite the secret key rate formula as

$$R^\infty = \frac{1}{2} \sum_{y \in \{q, p\}} p_{pass}^y \left\{ \min_{\rho_{AB} \in \mathbf{S}} H(\mathbf{Z}_y|E) - \delta_{EC}^y \right\}, \quad (4)$$

The coefficient $\frac{1}{2}$ represents half of states are measured in \hat{q} and half in \hat{p} . Note that Eve manipulates the density matrix ρ_{AB} without the knowledge of Bob's choice of quadrature when part of ρ_{AB} is in the quantum channel. We can move the summation sign into the minimization problem since ρ_{AB} of different quadratures are shared.

1. Knowledge of Eve

According to the Ref. [54, 55], the first term in formula (4) about the conditional entropy with the sifting probability can be reformulated as

$$\frac{1}{2} \min_{\rho_{AB} \in \mathbf{S}} \sum_{y \in \{q, p\}} D(\mathcal{G}_y(\rho_{AB}) || \mathcal{Z}[\mathcal{G}_y(\rho_{AB})]), \quad (5)$$

where $D(\rho || \sigma) = \text{Tr}(\rho \log_2 \rho) - \text{Tr}(\rho \log_2 \sigma)$ is the quantum relative entropy, \mathcal{G}_y describes the post-processing of different quadratures, \mathcal{Z} is a pinching quantum channel to read out the key information. The post-processing map $\mathcal{G}_y(\rho) = K_y \rho K_y^\dagger$ corresponds to the measurement $\hat{y} \in \{\hat{q}, \hat{p}\}$ and is given by

$$K_y = \sum_{b=0}^1 |b\rangle_R \otimes \mathbb{I}_A \otimes (\sqrt{I_y^b})_B, \quad (6)$$

where $|b\rangle_R$ is the state of the key register R , which is determined by interval operators I_y^b . $\{I_y^b\}$ project the system B into one of two subspaces spanned by the eigenstates of operator \hat{y} in terms of the mapping rule:

$$I_y^0 = \int_{\Delta}^{\infty} dy |y\rangle\langle y|, \quad I_y^1 = \int_{\infty}^{-\Delta} dy |y\rangle\langle y|. \quad (7)$$

$\mathcal{Z}(\rho) = \sum_{b=0}^1 Z_b \rho Z_b$ reads out the key from the mapping $\mathcal{G}_y(\rho_{AB})$ with $Z_0 = |0\rangle\langle 0|_R \otimes \mathbb{I}_{AB}$ and $Z_1 = |1\rangle\langle 1|_R \otimes \mathbb{I}_{AB}$. Here, \mathcal{G}_y is in a simplified form introduced by Ref. [38]. Kraus operators K_y describe the part of measurement and announcement. Alice announces nothing and has no effect of the register R . Therefore, Alice's operation is described by an identity matrix. Her measurement in entanglement-based protocol can be moved after

the announcement and never influences K_y . Bob would announce the choice of quadratures. We will discuss two quadratures separately, denoted by the parameter $y \in \{q, p\}$ in those formulas. His measurement is described by interval operators.

2. Error correction

Considering the reverse reconciliation, Alice corrects her string \mathbf{X} by leaking $H(\mathbf{Z}|\mathbf{X}) = H(\mathbf{Z}) - I(\mathbf{X}; \mathbf{Z})$ amount of information ideally. However, error correction cannot be as efficient as ideal. Parameter β is inserted before the mutual information term and then the leakage is

$$\begin{aligned} \delta_{EC}^y &= H(\mathbf{Z}_y) - \beta I(\mathbf{X}_y; \mathbf{Z}_y) \\ &= (1 - \beta)H(\mathbf{Z}_y) + \beta H(\mathbf{Z}_y|\mathbf{X}_y). \end{aligned} \quad (8)$$

Finally, the key rate formula is

$$\begin{aligned} R^\infty &= \frac{1}{2} \left\{ \min_{\rho_{AB} \in \mathbf{S}} \sum_{y \in \{q, p\}} D(\mathcal{G}_y(\rho_{AB}) || \mathcal{Z}[\mathcal{G}_y(\rho_{AB})]) \right. \\ &\quad \left. - \sum_{y \in \{q, p\}} p_{pass}^y \delta_{EC}^y \right\}. \end{aligned} \quad (9)$$

C. Numerical method

To realize the calculation of the secret key rates by computer, a photon-number cutoff assumption [38] is adopted. By this assumption, we can describe operators and density matrices in photon number representation with finite dimension. Since δ_{EC} and p_{pass} are only concerned with the information held by Alice and Bob, the calculation of the last term in key rate formula (9) is easy to implement. Numerical method is used for solving the rest part of the formula. Specifically, we calculate the minimization part in the formula by numerical method. The minimization problem can be described by

$$\text{minimize} \sum_{y \in \{q, p\}} D(\mathcal{G}_y(\rho_{AB}) || \mathcal{Z}[\mathcal{G}_y(\rho_{AB})])$$

subject to

$$\begin{aligned} \text{Tr}[\rho_{AB}(|x\rangle\langle x|_A \otimes \hat{q})] &= p_x \langle \hat{q} \rangle_x, \\ \text{Tr}[\rho_{AB}(|x\rangle\langle x|_A \otimes \hat{p})] &= p_x \langle \hat{p} \rangle_x, \\ \text{Tr}[\rho_{AB}(|x\rangle\langle x|_A \otimes \hat{n})] &= p_x \langle \hat{n} \rangle_x, \\ \text{Tr}[\rho_{AB}(|x\rangle\langle x|_A \otimes \hat{d})] &= p_x \langle \hat{d} \rangle_x, \\ \text{Tr}_B[\rho_{AB}] &= \sum_{i,j=0}^3 \sqrt{p_i p_j} \langle \alpha_j | \alpha_i \rangle |i\rangle\langle j|_A, \\ \text{Tr}[\rho_{AB}] &= 1, \\ \rho_{AB} &\geq 0. \end{aligned} \quad (10)$$

The variable is the density matrix ρ_{AB} subject to some constraints [38]. The first four constraints come from

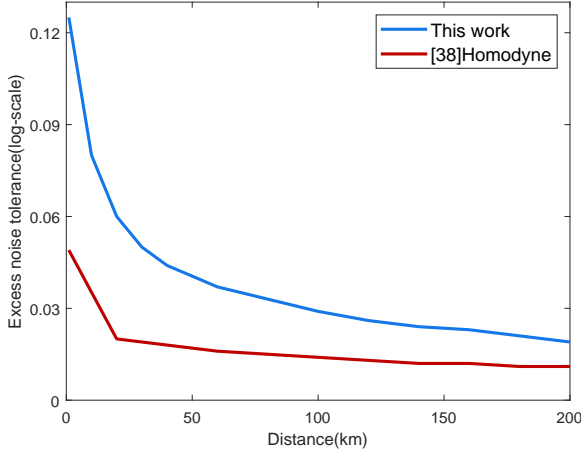


FIG. 3. The comparison between the excess noise tolerance of our protocol and that of protocol 1 in Ref. [38] with homodyne detection. The upper line is the performance of our protocol. The bottom line is the performance of compared protocol.

the experimental outcomes, where $x \in \{00, 10, 11, 01\}$ and $\langle \hat{q} \rangle_x, \langle \hat{p} \rangle_x, \langle \hat{n} \rangle_x, \langle \hat{d} \rangle_x$ are the expectation values of operators when Alice sends the states labeled by x . Homodyne detection directly outputs the outcomes of operators \hat{q} and \hat{p} , while $\hat{n} = \frac{1}{2}(\hat{q}^2 + \hat{p}^2 - 1)$ and $\hat{d} = \hat{q}^2 - \hat{p}^2$ correspond to the second moments of \hat{q} and \hat{p} , and is indirectly given by homodyne detection. Next constraint about partial trace of system B comes from the requirement of CPTP mapping, which means that the quantum channel can not influence the system A of Alice. Last two constraints are natural requirements since ρ_{AB} is a density matrix.

This minimization problem can be solved in many ways. We adopt one use linearization method, given in Appendix. A.

IV. PERFORMANCE

Here, we investigate the performance of our protocol by numerical simulation. The method of simulation is mentioned in Appendix. B.

Excess noise tolerance is calculated by maximizing the excess noise ξ at a distance. As shown in Fig. 3, our protocol shows significantly higher tolerance of excess noise compared with the previous homodyne protocol [38].

To investigate the best performance of our protocol under different distances, we optimize the amplitude α of signal states in the interval $[0.6, 1.1]$ with step of 0.01.

We emphasize the remarkable excess noise tolerance of our protocol. The compared protocol [38] prepares states with phases $\{0, \frac{\pi}{2}, \pi, \frac{3\pi}{2}\}$ and uses sending states with phase 0 and π to generate key. We optimize the amplitude α of compared protocol in the range $[0.35, 0.6]$ with step of 0.01, as mentioned in reference. Different

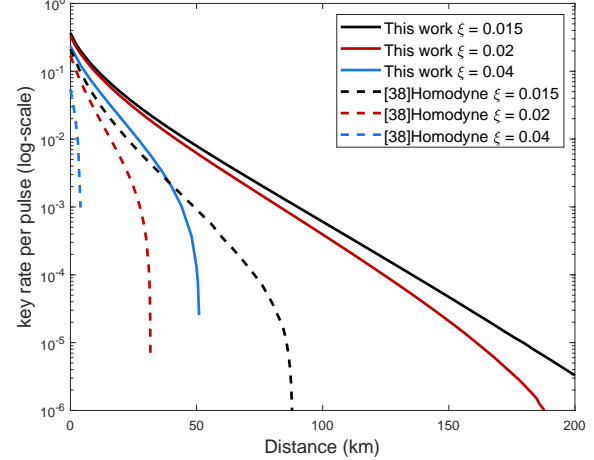


FIG. 4. The comparison between the secret key rates of our protocol and that of protocol 1 in Ref. [38] with homodyne detection. The solid lines from top to bottom are the performance of our protocol under excess noise $\xi = 0.015, 0.02, 0.04$. The dashed lines from top to bottom are the performance of compared protocol under excess noise $\xi = 0.015, 0.02, 0.04$.

search ranges are used because the optimal range of α may vary for different protocols. In Fig. 4, the solid lines correspond to the key rates of our protocol for different excess noises. The dashed lines show the performance of compared protocol. When the excess noise adopts experimental parameters such as $\xi = 0.02$, our protocol enables to distribute keys around 200 km with meaningful 10^{-6} bit per pulse secret key rate. Moreover, when compared protocol can hardly generate keys for $\xi = 0.04$, our protocol can still distribute secret keys over 50 km.

Further, we show the improvement of transmission distance even happens for the small excess noise, as shown in Fig. 5. When the excess noise is sufficiently small, our protocol has potential to distribute secret keys over 360 km. The transmission distance and secret key rates are increased a lot, which makes our protocol applicable and useful in the quantum secure communication network.

Note that the curve should have been smooth in theory. However, as a numerical method, limited by the calculation accuracy of computers and the stability of convex optimization algorithm, unstable points and unsmooth curves appear. The quality of the algorithm largely determines the secret key rates. When ideal secret key rate is so small that reaches the calculating accuracy of computer, the numerical results sometimes show no key can be generated. The calculation speed of the numerical method is usually terribly slow with perhaps 20 min per set of parameters. The improvement of the algorithm may help to further improve the transmission distance and stabilize the key rates.

To give suggestions for experiments, we show the optimal amplitudes searched in different transmission distances. As shown in Fig. 6, the optimal amplitude de-

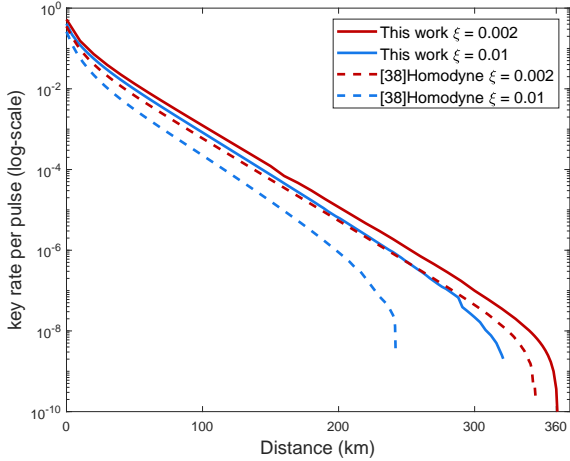


FIG. 5. The comparison between the secret key rates of our protocol and that of protocol 1 in Ref. [38] with homodyne detection. The solid lines from top to bottom are the performance of our protocol under excess noise $\xi = 0.002, 0.005, 0.01$. The dashed lines from top to bottom are the performance of compared protocol under excess noise $\xi = 0.002, 0.005, 0.01$.

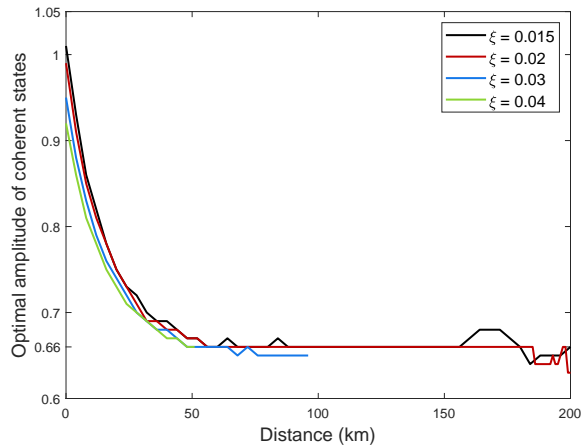


FIG. 6. The optimal amplitudes of the coherent states prepared by Alice in different transmission distances. From top to bottom, the lines correspond to the conditions that the excess noises are $\xi = 0.015, 0.02, 0.03, 0.04$.

creases with the transmission distance increasing, except some jitters in long distances. And the smaller excess noise has lower optimal amplitude with little violation in long distances. The jitter of the optimal amplitudes in long distances is due to the imprecision of the numerical calculation on computer. Although the secret key rate formula is a convex function with convex domain ρ_{AB} in theory, the imprecision of ρ_{AB} satisfying the constraints is difficult to be unified under different amplitude and transmittance. The calculation inaccuracy also accumulates along with steps of calculations, which results in

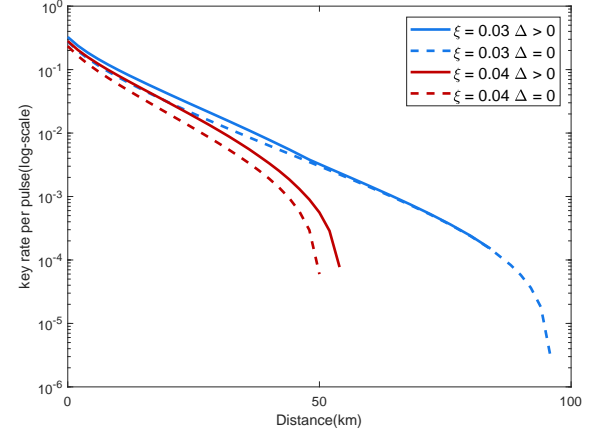


FIG. 7. The performance of the optimal post-selection. Two conditions with different excess noises $\xi = 0.03$ and $\xi = 0.04$ are considered. The top solid line in red represents the performance of the post-selection with $\xi = 0.03$, while the lower solid line in blue is the performance without post-selection. The top dash line in red represents the performance of the post-selection $\xi = 0.04$, while the lower solid line in blue is the performance without post-selection.

some calculation noise. At long distance, the key rate gradually approaches the magnitude of the calculation noise, thus the convexity of the key rate can be violated in a small range of amplitude. The optimal amplitude for remote users is about 0.66 in Fig. 6.

Post-selection is a useful method to further improve the transmission distance. We optimize sifting parameter Δ of post-selection with the amplitude of the coherent state that has been optimized without post-selection. The interval of the available Δ is 0.01. At the distance where the secret key rates are zeros without post-selection, we search the best post-selection parameter Δ by setting the optimal amplitude 0.66. This choice is reasonable considering that the optimal amplitude in long distance is around 0.66 in average, as shown in Fig. 6. In Fig. 7, the secret key rates are improved at most distance, and the largest transmission distance for $\xi = 0.04$ is even extended. Thus the post-selection makes sense in our protocol. However, at the optimal amplitude, the improvement of post-selection is a little small for $\xi = 0.03$. When distance is large, it shows no improvement of secret key rates. This operation can work well when the amplitude cannot be prepared optimally in experiment.

V. DISCUSSION

Homodyne detection is the first adopted measurement method of CV-QKD with good performance in experiment. Homodyne detection shows great tolerance of excess noise in Gaussian-modulated protocols. Moreover, homodyne detection is superior to heterodyne detection

in experiment, since the latter introduces additional vacuum noise required by uncertainty relation and requires two homodyne detectors being balanced. It is a pity that the quaternary-modulated CV-QKD protocol with homodyne detection, which works like a two-dimensional DV-QKD protocol with biased selection of measurement bases, shows obviously inferiority compared with heterodyne detection [38]. What makes homodyne detection protocol show much lower excess noise tolerance than heterodyne detection protocol? To answer this question and to preserve the experimental advantage of homodyne detector, we provide a new homodyne detection CV-QKD protocol applying QPSK to preparation. The first difference is that, as we mentioned in our protocol, Alice prepares states with two-bit information. Nevertheless, with one homodyne detector, Bob can randomly choose one bit for each round. In this aspect, it is similar to a heterodyne detection randomly discarding one bit in each round. Conceptually, this kind of discarding is equivalent to dividing the secret key rate by 2, which only causes the decrease of the secret key rate but has no influence in the transmission distance.

A subproblem rises: why previous homodyne detection protocols cannot transmit in long distance since they also send four kinds of states. Especially, from a practical point of view, our protocol and previous protocols all generate one bit per pulse. As we can see, Alice keeps silence in our protocol, while Alice announces the basis of sending states in previous protocols. In fact, wonderful excess noise tolerance is obviously not due to the difference of measurement operators. It comes from the less information leakage. Biased selection in previous protocol only increases the number of rounds for distill key, having done nothing about the information leakage.

Another subproblem is: why we adopt QPSK in preparation. Note that QPSK is a mature method in classical communication, shifting the phase of states by $\{\frac{\pi}{4}, \frac{3\pi}{4}, \frac{5\pi}{4}, \frac{7\pi}{4}\}$. In previous quaternary-modulated protocols [37, 38], they use the states with phases $\{0, \frac{\pi}{2}, \pi, \frac{3\pi}{2}\}$. Thus a $\frac{\pi}{4}$ phase shift in preparation is involved. Without doubt, $\frac{\pi}{4}$ phase shift is necessary in our protocol, since it offers chance to generate key in both quadratures. If a state has phase 0 or π , the probability distribution of state in quadrature \hat{p} is symmetric about 0. Thus the states with phase 0 or π cannot represent keys when Bob applies \hat{p} . At the same time, the states with $\frac{\pi}{2}$ or $\frac{3\pi}{2}$ cannot represent keys when Bob applies \hat{q} . Therefore, huge difference happens. Our QPSK protocol allows high excess noise just like what heterodyne detection protocols do, even though homodyne detection is applied.

Eventually, due to the tolerance of excess noise, the transmission distances are improved, which removes the obstruction of the proceedings of large-scale discrete-modulated CV-QKD network. It is worth recalling that commercial instruments for QPSK have been updated to over 50Gbps [56], which implies that the speed of preparation in our protocol is also promoted to 50Gbps.

Our protocol will make full use of the superior performance of the homodyne detector to achieve the long distance key distribution similar to the theoretical results of heterodyne detection protocols. It is of great practical value for the network security and information security to experimentally demonstrate our protocol. With simpler preparation, our protocol has chance to exceed the transmission record 202.81 km set by Gaussian modulation protocol [57] with ultralow-loss fiber and other good conditions. The experimental schematic and the search of optimal amplitude in the text provide references for the experimental implementation.

Further study of our protocol's security is also desirable. Note that the photon-number cutoff assumption can be removed [58] in heterodyne detection protocol, which inspires our protocol to stricter security in the future work. Moreover, we can put our efforts in finding the proper adjustment of security theory to deal with the finite-size effects. The security against coherent attacks is another interesting and important direction for developing discrete-modulated CV-QKD. The quantum de Finetti representation theorem [59] is a possible path to equalize the information leaked by coherent attacks and collective attacks. Our converting idea may still be available because it has nothing to do with permutation invariance in the quantum de Finetti representation theorem.

ACKNOWLEDGMENTS

We gratefully acknowledge support from the National Natural Science Foundation of China (under Grant No. 61801420); the Key-Area Research and Development Program of Guangdong Province (under Grant No. 2020B0303040001); the Fundamental Research Funds for the Central Universities.

Appendix A: Numerical methods of calculating the key rates

The minimization problem in Eq. (10) is a convex optimal problem with one unique solution. It can be described as follows:

The independent variable is the density matrix ρ_{AB} . The dimension of Alice's system is 4, which is determined by the number of different states she prepared. $|x\rangle\langle x|_A$ with $x \in \{00, 10, 11, 01\}$ projects Alice's system into a one-dimensional subspace, which means that Alice sends state $|\phi_x\rangle \in \left\{ \left| \alpha e^{i\frac{\pi}{4}} \right\rangle, \left| \alpha e^{i\frac{3\pi}{4}} \right\rangle, \left| \alpha e^{i\frac{5\pi}{4}} \right\rangle, \left| \alpha e^{i\frac{7\pi}{4}} \right\rangle \right\}$ to Bob. The state Bob receives, however, is infinite-dimensional. The photon-number cutoff assumption is proposed to cut off the dimension of Bob's system. According to the assumption, ρ_{AB} can be represented by a finite-dimensional matrix in Fock representation. Thus numerical method can be applied. The operators $\hat{q}, \hat{p}, \hat{n}, \hat{d}$ correspond to the

measurement on Bob's system. Considering the photon-number representation, they can be defined by the annihilation operator \hat{a} :

$$\begin{aligned}\hat{q} &= \frac{1}{\sqrt{2}}(\hat{a} + \hat{a}^\dagger), \\ \hat{p} &= \frac{i}{\sqrt{2}}(\hat{a}^\dagger - \hat{a}), \\ \hat{n} &= \hat{a}^\dagger \hat{a} = \hat{a} \hat{a}^\dagger - 1, \\ \hat{d} &= \hat{a}^2 + (\hat{a}^\dagger)^2.\end{aligned}\quad (\text{A1})$$

To calculate them numerically, the matrix of \hat{a} in photon-number representation is also cut off according to the photon-number cutoff assumption. We introduce notations $\langle \hat{q} \rangle_x, \langle \hat{p} \rangle_x, \langle \hat{n} \rangle_x, \langle \hat{d} \rangle_x$ to represent the expectation values of these operators. The relative entropy $D(\rho || \sigma)$ is the dependent variable we need to minimize. $\mathcal{G}(\rho) = K\rho K^\dagger$ is the map in post-processing with Kraus operator K .

To implement the convex optimization, a two-step numerical method is introduced [55] below. To be convenient, we use $f(\rho)$ to represent the function $D(\mathcal{G}(\rho) || \mathcal{Z}[\mathcal{G}(\rho)])$. The constraints can be described by a set \mathcal{S} :

$$\mathcal{S} = \{\rho \in \mathcal{H}_+ | Tr(\Gamma_i \rho) = \gamma_i, \forall i\}, \quad (\text{A2})$$

where \mathcal{H}_+ is the set of positive semidefinite operators. Γ_i is Hermitian operator and γ_i is the corresponding expectation value. To fit in this form, one should rewrite the fifth constraint in Eq. (10). Specifically one need transform partial trace on Bob into some Hermitian operators.

Through linearization method, we can get

$$\begin{aligned}f(\rho^*) &\geq f_\epsilon(\rho) + \min_{\rho + \Delta\rho \in \mathcal{S}} [Tr((\Delta\rho)^T \nabla f_\epsilon(\rho))] - \zeta_\epsilon, \\ &= f_\epsilon(\rho) - Tr(\rho^T \nabla f_\epsilon(\rho)) + \min_{\sigma \in \mathcal{S}} [Tr(\sigma^T \nabla f_\epsilon(\rho))] - \zeta_\epsilon,\end{aligned}\quad (\text{A3})$$

where ρ^* is the optimal density matrix, i.e. the solution of minimization problem Eq. (10). ϵ represents a perturbation parameter, by which the gradient of $f(\rho)$ can exist. Due to the existence of ϵ , the term $\zeta_\epsilon = 2\epsilon(d' - 1) \log_2 \frac{d'}{\epsilon(d'-1)}$ is applied to correct the difference between $f(\rho)$ and $f_\epsilon(\rho)$ caused by perturbation. In our simulation, we set $\epsilon = 10^{-12}$ to decrease the value of ζ_ϵ . With ϵ , the dependent variable becomes

$$f_\epsilon(\rho) = D(\mathcal{G}_\epsilon(\rho) || \mathcal{Z}[\mathcal{G}_\epsilon(\rho)]). \quad (\text{A4})$$

The gradient of $f_\epsilon(\rho)$ is

$$[\nabla f_\epsilon(\rho)]^T = \mathcal{G}_\epsilon^\dagger(\log_2 \mathcal{G}_\epsilon(\rho)) - \mathcal{G}_\epsilon^\dagger(\log_2 \mathcal{Z}(\mathcal{G}_\epsilon(\rho))), \quad (\text{A5})$$

in which

$$\begin{aligned}\mathcal{G}_\epsilon(\rho) &= (1 - \epsilon)\mathcal{G}(\rho) + \epsilon \mathbb{I} / d', \\ \mathcal{Z}(\mathcal{G}_\epsilon(\rho)) &= (1 - \epsilon)\mathcal{Z}(\mathcal{G}(\rho)) + \epsilon \mathbb{I} / d'.\end{aligned}\quad (\text{A6})$$

d' is the dimension of the matrix $\mathcal{G}(\rho)$, which is twice the dimension of density matrix ρ .

Through the linearization showed in Eq. (A3), the optimization problem is transformed into a semi-definite program, such as the second term of the first line or the third term of the second line in Eq. (A3). Therefore, we only need to find $\Delta\rho$ or $\sigma = \rho + \Delta\rho$ that minimizes the related term. We take $\Delta\rho$ for example, the first step is to find a density matrix ρ that is very close to the optimal one. To accomplish this step, we perform algorithm as follows:

1. Begin with any $\rho_0 \in \mathcal{S}$ and set $i = 0$.
2. Compute $\min_{\rho + \Delta\rho \in \mathcal{S}} [Tr((\Delta\rho)^T \nabla f_\epsilon(\rho_i))]$.
3. If $Tr((\Delta\rho)^T \nabla f_\epsilon(\rho_i))$ is sufficiently small, STOP.
4. Find $\lambda \in (0, 1)$ that minimizes $f_\epsilon(\rho_i + \lambda \Delta\rho)$.
5. Set $\rho_{i+1} = \rho_i + \lambda \Delta\rho$, $i \leftarrow i + 1$ and go to 2.

The iteration of 2-5 sometimes needs to be broken manually otherwise it may take too much time to converge or even never stop. The largest iteration number in our simulation is 300. After 300 iterations we choose ρ_i with the smallest $Tr((\Delta\rho)^T \nabla f_\epsilon(\rho_i))$ among all iterations as our result of the first step.

The reference [55] does not offer any method to deal with the minimization of $f_\epsilon(\rho_i + \lambda \Delta\rho)$, since its DV-QKD example is simple for calculation. However, it is not an easy task for CV-QKD. We provide our own method inspired by BinarySearch:

1. Set starting point $\lambda_s = 0$, ending point $\lambda_e = 1$ and middle point $\lambda_m = 0.5$.
2. Calculate $f_\epsilon(\rho_i + \lambda \Delta\rho)$ in three points and compare them.
3. If starting point is the smallest one, update ending point by $\lambda_e = \lambda_m$ and middle point by $\lambda_m = 0.5(\lambda_s + \lambda_e)$. Then go to 2.
4. If ending point is the smallest one, update starting point by $\lambda_s = \lambda_m$ and middle point by $\lambda_m = 0.5(\lambda_s + \lambda_e)$. Then go to 2.
5. If middle point is the smallest one, two temporary points are generated by $\lambda_1 = 0.5(\lambda_s + \lambda_m)$ and $\lambda_2 = 0.5(\lambda_m + \lambda_e)$.
6. Calculate $f_\epsilon(\rho_i + \lambda \Delta\rho)$ of two temporary points and compare them with λ_m .
7. If middle point is still the smallest one, set $\lambda_s = \lambda_1$ and $\lambda_e = \lambda_2$ and go to 2.
8. If temporary point λ_1 is the smallest one, set $\lambda_e = \lambda_m$ and $\lambda_m = \lambda_1$ and go to 2.
9. If temporary point λ_2 is the smallest one, set $\lambda_s = \lambda_m$ and $\lambda_m = \lambda_2$ and go to 2.

The calculation results of some points can be temporarily stored for next iteration. The termination of the iteration is decided by the calculation accuracy of computer.

After first step, we seemingly find an appropriate density matrix ρ . However, considering the imprecision of numerical calculation, we can not guarantee the solution of first step is the optimal one. In fact, we find an upper bound of the solution. To protect the security of the generated key, we use the dual problem in the second

step.

One can transform the primal problem $\min_{\sigma \in \mathbf{S}} [Tr(\sigma^T \nabla f_\epsilon(\rho))]$ into dual problem $\max_{\vec{y} \in \mathbf{S}^*(\rho)} \vec{\gamma} \cdot \vec{y}$. The variable \vec{y} obeys the constraints:

$$\mathbf{S}^*(\rho) = \{\vec{y} \in \mathbb{R}^n \mid \sum_i y_i \Gamma_i^T \leq \nabla f_\epsilon(\rho)\}. \quad (\text{A7})$$

In general, primal and dual problems satisfy the weak duality. The weak duality emphasizes the optimal value of dual problem is always less than or equal to the optimal value of primal problem. According to this principle, the final solution we obtain from the dual problem must be a lower bound of the primal problem even if it is not optimal. The lower bound of the primal problem is also the lower bound of the secret key rates according to Eq. (A3).

Additionally, we can consider the imprecision of the floating-point representations of $\{\Gamma_i\}$ and $\{\gamma_i\}$.

$$|Tr(\tilde{\Gamma}_i \rho) - \tilde{\gamma}_i| \leq \epsilon_{rep}, \quad (\text{A8})$$

where $\{\tilde{\Gamma}_i\}$ and $\{\tilde{\gamma}_i\}$ are the approximate representations used in calculation. Furthermore, the solution ρ may not satisfy the constraints, especially the positive semi-definite constraint. The reference [55] encourages one to transform ρ into positive semi-definite matrix ρ' by subtracting a term $\lambda_{min} \mathbb{I}$ when the smallest eigenvalue λ_{min} of ρ is negative. Then we restrict the imprecision by

$$|Tr(\tilde{\Gamma}_i \rho') - \tilde{\gamma}_i| \leq \epsilon_{sol}. \quad (\text{A9})$$

After the first step, we extract the quantity $\epsilon' = \max(\epsilon_{rep}, \epsilon_{sol})$ from the output ρ . This quantity influences the second step. The dual problem solved in second step is adjusted to

$$\max_{(\vec{y}, \vec{z}) \in \tilde{\mathbf{S}}^*(\rho)} \left(\vec{\gamma} \cdot \vec{y} - \epsilon' \sum_{i=1}^n z_i \right), \quad (\text{A10})$$

where

$$\begin{aligned} \tilde{\mathbf{S}}^*(\rho) &:= \{(\vec{y}, \vec{z}) \in (\mathbb{R}^n, \mathbb{R}^n) \mid -\vec{z} \leq \vec{y} \leq \vec{z}, \sum_i y_i \tilde{\Gamma}_i^T \leq \nabla f_\epsilon(\rho)\}. \end{aligned} \quad (\text{A11})$$

The description above is about one quadrature. Since $f_q(\rho)$ for \hat{q} and $f_p(\rho)$ for \hat{p} are added linearly, we can replace $f_\epsilon(\rho)$ by $f_{q,\epsilon}(\rho) + f_{p,\epsilon}(\rho)$. Then $\nabla f_\epsilon(\rho)$ in primal and dual problem is replaced by $\nabla f_{q,\epsilon}(\rho) + \nabla f_{p,\epsilon}(\rho)$. Additionally, the perturbation compensation ζ_ϵ is multiplied by 2.

So far, the lower bound of the minimization problem is solved numerically. We can solve the primal and dual problems by the SDPT3 solver in CVX package.

Appendix B: Methods of simulation

We simulate the experiment statistical results by supposing a phase-invariant Gaussian channel, as referred in Ref. [38]. When Alice sends a coherent state $|\alpha\rangle$, Bob obtains a displaced thermal state centered at $\sqrt{\eta}\alpha$ with the variance $\frac{1}{2} + \frac{\eta\xi}{2}$ for each quadrature. The first term $\frac{1}{2}$ in the variance is the vacuum noise. Thus ρ_B^x can be given by

$$\rho_B^x = \frac{1}{\pi V_A} \int e^{-|\beta - \sqrt{\eta}\alpha_x|^2/V_A} |\beta\rangle\langle\beta| d^2\beta, \quad (\text{B1})$$

with $\alpha_x \in \{|\alpha e^{i\frac{\pi}{4}}\rangle, |\alpha e^{-i\frac{\pi}{4}}\rangle, |\alpha e^{i\frac{3\pi}{4}}\rangle, |\alpha e^{i\frac{5\pi}{4}}\rangle\}$ and $V_A = \frac{\eta\xi}{2}$. ξ is the excess noise and $\eta = 10^{-\frac{aL}{10}}$ is the transmittance with $a = 0.2$ dB/km in the distance L . Thus the expect values of operators are

$$\begin{aligned} \langle \hat{q} \rangle_x &= \sqrt{2\eta} Re(\alpha_x), \\ \langle \hat{p} \rangle_x &= \sqrt{2\eta} Im(\alpha_x), \\ \langle \hat{n} \rangle_x &= \eta|\alpha_x|^2 + \frac{\eta\xi}{2}, \\ \langle \hat{d} \rangle_x &= \eta[(\alpha_x)^2 + (\alpha_x^*)^2]. \end{aligned} \quad (\text{B2})$$

In order to simulate the error-correction, the conditional probability between Alice's sending state and Bob's mapping result can be given by:

$$P(q|x) = \frac{1}{\sqrt{\pi(\eta\xi+1)}} e^{[-(q - \sqrt{2\eta} Re(\alpha_x))^2]/(\eta\xi+1)}, \quad (\text{B3})$$

for measuring \hat{q} .

$$P(p|x) = \frac{1}{\sqrt{\pi(\eta\xi+1)}} e^{[-(p - \sqrt{2\eta} Im(\alpha_x))^2]/(\eta\xi+1)} \quad (\text{B4})$$

for measuring \hat{p} . According to the bit mapping of Bob, the probability distribution of the bit is

$$\begin{aligned} P_y(0|x) &= \int_{\Delta}^{\infty} P(y|x) dy, \\ P_y(1|x) &= \int_{-\infty}^{\Delta} P(y|x) dy, \\ P_y(\perp|x) &= \int_{-\Delta}^{\Delta} P(y|x) dy, \end{aligned} \quad (\text{B5})$$

where $y \in \{q, p\}$. Then we can find the sifting probability

$$P_{pass}^y = \sum_x p_x (P_y(0|x) + P_y(1|x)), \quad (\text{B6})$$

and normalize the probability distribution after discarding bits \perp . The conditional entropy for each quadrature is thus calculated by

$$H(\mathbf{Z}_y|\mathbf{X}_y) = - \sum_x p_x \sum_{z \in \{0,1\}} \frac{P_y(z|x)}{P_{pass}^y} \log_2 \frac{P_y(z|x)}{P_{pass}^y}. \quad (\text{B7})$$

By utilizing the equations above, the experiment results required by calculating the key rates have been simulated.

[1] F. Arute, K. Arya, R. Babbush, D. Bacon, J. C. Bardin, R. Barends, R. Biswas, S. Boixo, F. G. Brandao, D. A. Buell, *et al.*, Quantum supremacy using a programmable superconducting processor, *Nature* **574**, 505 (2019).

[2] H.-S. Zhong, H. Wang, Y.-H. Deng, M.-C. Chen, L.-C. Peng, Y.-H. Luo, J. Qin, D. Wu, X. Ding, Y. Hu, *et al.*, Quantum computational advantage using photons, *Science* **370**, 1460 (2020).

[3] R. L. Rivest, A. Shamir, and L. Adleman, A method for obtaining digital signatures and public-key cryptosystems, *Commun. of the ACM* **21**, 120 (1978).

[4] P. W. Shor, Algorithms for quantum computation: discrete logarithms and factoring, in *Proceedings 35th Annual Symposium on Foundations of Computer Science* (IEEE, 1994) pp. 124–134.

[5] C. E. Shannon, Communication theory of secrecy systems, *The Bell System Technical Journal* **28**, 656 (1949).

[6] C. H. Bennett and G. Brassard, Quantum cryptography: Public key distribution and coin tossing, in *Proceedings of the IEEE International Conference on Computers, Systems and Signal Processing* (1984).

[7] A. K. Ekert, Quantum cryptography based on bell's theorem, *Phys. Rev. Lett.* **67**, 661 (1991).

[8] C. Weedbrook, S. Pirandola, R. García-Patrón, N. J. Cerf, T. C. Ralph, J. H. Shapiro, and S. Lloyd, Gaussian quantum information, *Rev. Mod. Phys.* **84**, 621 (2012).

[9] S. Pirandola, U. L. Andersen, L. Banchi, M. Berta, D. Bunandar, R. Colbeck, D. Englund, T. Gehring, C. Lupo, C. Ottaviani, J. L. Pereira, M. Razavi, J. S. Shaari, M. Tomamichel, V. C. Usenko, G. Vallone, P. Villoresi, and P. Wallden, Advances in quantum cryptography, *Adv. Opt. Photon.* **12**, 1012 (2020).

[10] F. Xu, X. Ma, Q. Zhang, H.-K. Lo, and J.-W. Pan, Secure quantum key distribution with realistic devices, *Rev. Mod. Phys.* **92**, 025002 (2020).

[11] Y. Zhao, B. Qi, X. Ma, H.-K. Lo, and L. Qian, Experimental quantum key distribution with decoy states, *Phys. Rev. Lett.* **96**, 070502 (2006).

[12] L. Comandar, M. Lucamarini, B. Fröhlich, J. Dynes, A. Sharpe, S.-B. Tam, Z. Yuan, R. Penty, and A. Shields, Quantum key distribution without detector vulnerabilities using optically seeded lasers, *Nat. Photonics* **10**, 312 (2016).

[13] K. Wei, W. Li, H. Tan, Y. Li, H. Min, W.-J. Zhang, H. Li, L. You, Z. Wang, X. Jiang, T.-Y. Chen, S.-K. Liao, C.-Z. Peng, F. Xu, and J.-W. Pan, High-speed measurement-device-independent quantum key distribution with integrated silicon photonics, *Phys. Rev. X* **10**, 031030 (2020).

[14] H.-L. Yin, T.-Y. Chen, Z.-W. Yu, H. Liu, L.-X. You, Y.-H. Zhou, S.-J. Chen, Y. Mao, M.-Q. Huang, W.-J. Zhang, H. Chen, M. J. Li, D. Nolan, F. Zhou, X. Jiang, Z. Wang, Q. Zhang, X.-B. Wang, and J.-W. Pan, Measurement-device-independent quantum key distribution over a 404 km optical fiber, *Phys. Rev. Lett.* **117**, 190501 (2016).

[15] A. Boaron, G. Boso, D. Rusca, C. Vulliez, C. Autebert, M. Caloz, M. Perrenoud, G. Gras, F. Bussières, M.-J. Li, D. Nolan, A. Martin, and H. Zbinden, Secure quantum key distribution over 421 km of optical fiber, *Phys. Rev. Lett.* **121**, 190502 (2018).

[16] H.-L. Yin, P. Liu, W.-W. Dai, Z.-H. Ci, J. Gu, T. Gao, Q.-W. Wang, and Z.-Y. Shen, Experimental composable security decoy-state quantum key distribution using time-phase encoding, *Opt. Express* **28**, 29479 (2020).

[17] Y.-L. Tang, H.-L. Yin, Q. Zhao, H. Liu, X.-X. Sun, M.-Q. Huang, W.-J. Zhang, S.-J. Chen, L. Zhang, L.-X. You, Z. Wang, Y. Liu, C.-Y. Lu, X. Jiang, X. Ma, Q. Zhang, T.-Y. Chen, and J.-W. Pan, Measurement-device-independent quantum key distribution over untrustful metropolitan network, *Phys. Rev. X* **6**, 011024 (2016).

[18] E. Diamanti and A. Leverrier, Distributing secret keys with quantum continuous variables: Principle, security and implementations, *Entropy* **17**, 6072 (2015).

[19] F. Grosshans and P. Grangier, Continuous variable quantum cryptography using coherent states, *Phys. Rev. Lett.* **88**, 057902 (2002).

[20] F. Grosshans, G. Van Assche, J. Wenger, R. Brouri, N. J. Cerf, and P. Grangier, Quantum key distribution using gaussian-modulated coherent states, *Nature* **421**, 238 (2003).

[21] N. J. Cerf, M. Levy, and G. Van Assche, Quantum distribution of gaussian keys using squeezed states, *Phys. Rev. A* **63**, 052311 (2001).

[22] H.-L. Yin, W. Zhu, and Y. Fu, Phase self-aligned continuous-variable measurement-device-independent quantum key distribution, *Sci. Rep.* **9**, 49 (2019).

[23] C. Silberhorn, T. C. Ralph, N. Lütkenhaus, and G. Leuchs, Continuous variable quantum cryptography: Beating the 3 db loss limit, *Phys. Rev. Lett.* **89**, 167901 (2002).

[24] R. García-Patrón and N. J. Cerf, Continuous-variable quantum key distribution protocols over noisy channels, *Phys. Rev. Lett.* **102**, 130501 (2009).

[25] A. Leverrier, F. Grosshans, and P. Grangier, Finite-size analysis of a continuous-variable quantum key distribution, *Phys. Rev. A* **81**, 062343 (2010).

[26] A. Leverrier, Composable security proof for continuous-variable quantum key distribution with coherent states, *Phys. Rev. Lett.* **114**, 070501 (2015).

[27] C. Lupo, Towards practical security of continuous-variable quantum key distribution, *Phys. Rev. A* **102**, 022623 (2020).

[28] J. Lodewyck, M. Bloch, R. García-Patrón, S. Fossier, E. Karpov, E. Diamanti, T. Debuisschert, N. J. Cerf, R. Tualle-Brouri, S. W. McLaughlin, and P. Grangier, Quantum key distribution over 25 km with an all-fiber continuous-variable system, *Phys. Rev. A* **76**, 042305 (2007).

[29] B. Qi, L.-L. Huang, L. Qian, and H.-K. Lo, Experimental study on the gaussian-modulated coherent-state quantum key distribution over standard telecommunication fibers, *Phys. Rev. A* **76**, 052323 (2007).

[30] S. Fossier, E. Diamanti, T. Debuisschert, A. Villing, R. Tualle-Brouri, and P. Grangier, Field test of a continuous-variable quantum key distribution prototype, *New J. Phys.* **11**, 045023 (2009).

[31] G. Zhang, J. Y. Haw, H. Cai, F. Xu, S. Assad, J. F. Fitzsimons, X. Zhou, Y. Zhang, S. Yu, J. Wu, *et al.*, An integrated silicon photonic chip platform for continuous-variable quantum key distribution, *Nat. Photonics* **13**, 839 (2019).

[32] A. Leverrier and P. Grangier, Unconditional security proof of long-distance continuous-variable quantum key distribution with discrete modulation, *Phys. Rev. Lett.* **102**, 180504 (2009).

[33] Q. D. Xuan, Z. Zhang, and P. L. Voss, A 24 km fiber-based discretely signaled continuous variable quantum key distribution system, *Opt. Express* **17**, 24244 (2009).

[34] T. Hirano, T. Ichikawa, T. Matsubara, M. Ono, Y. Oguri, R. Namiki, K. Kasai, R. Matsumoto, and T. Tsurumaru, Implementation of continuous-variable quantum key distribution with discrete modulation, *Quantum Sci. Technol.* **2**, 024010 (2017).

[35] J. Lin and N. Lütkenhaus, Trusted detector noise analysis for discrete modulation schemes of continuous-variable quantum key distribution, *Phys. Rev. Applied* **14**, 064030 (2020).

[36] M. Ghalaii, C. Ottaviani, R. Kumar, S. Pirandola, and M. Razavi, Discrete-modulation continuous-variable quantum key distribution enhanced by quantum scissors, *IEEE J. Sel. Areas Commun.* **38**, 506 (2020).

[37] S. Ghorai, P. Grangier, E. Diamanti, and A. Leverrier, Asymptotic security of continuous-variable quantum key distribution with a discrete modulation, *Phys. Rev. X* **9**, 021059 (2019).

[38] J. Lin, T. Upadhyaya, and N. Lütkenhaus, Asymptotic security analysis of discrete-modulated continuous-variable quantum key distribution, *Phys. Rev. X* **9**, 041064 (2019).

[39] H. Hu, J. Im, J. Lin, N. Lütkenhaus, and H. Wolkowicz, Robust interior point method for quantum key distribution rate computation (2021), arXiv:2104.03847.

[40] A. Denys, P. Brown, and A. Leverrier, Explicit asymptotic secret key rate of continuous-variable quantum key distribution with an arbitrary modulation (2021), arXiv:2103.13945.

[41] P. Jouguet, S. Kunz-Jacques, A. Leverrier, P. Grangier, and E. Diamanti, Experimental demonstration of long-distance continuous-variable quantum key distribution, *Nat. Photonics* **7**, 378 (2013).

[42] S. Pirandola, C. Ottaviani, G. Spedalieri, C. Weedbrook, S. L. Braunstein, S. Lloyd, T. Gehring, C. S. Jacobsen, and U. L. Andersen, High-rate measurement-device-independent quantum cryptography, *Nat. Photonics* **9**, 397 (2015).

[43] D. Huang, P. Huang, D. Lin, C. Wang, and G. Zeng, High-speed continuous-variable quantum key distribution without sending a local oscillator, *Opt. Lett.* **40**, 3695 (2015).

[44] B. Qi, P. Lougovski, R. Pooser, W. Grice, and M. Bobrek, Generating the local oscillator “locally” in continuous-variable quantum key distribution based on coherent detection, *Phys. Rev. X* **5**, 041009 (2015).

[45] D. B. S. Soh, C. Brif, P. J. Coles, N. Lütkenhaus, R. M. Camacho, J. Urayama, and M. Sarovar, Self-referenced continuous-variable quantum key distribution protocol, *Phys. Rev. X* **5**, 041010 (2015).

[46] D. Huang, P. Huang, D. Lin, and G. Zeng, Long-distance continuous-variable quantum key distribution by controlling excess noise, *Sci. Rep.* **6**, 19201 (2016).

[47] W. Liu, Y. Cao, X. Wang, and Y. Li, Continuous-variable quantum key distribution under strong channel polarization disturbance, *Phys. Rev. A* **102**, 032625 (2020).

[48] C. Weedbrook, A. M. Lance, W. P. Bowen, T. Symul, T. C. Ralph, and P. K. Lam, Quantum cryptography without switching, *Phys. Rev. Lett.* **93**, 170504 (2004).

[49] A. M. Lance, T. Symul, V. Sharma, C. Weedbrook, T. C. Ralph, and P. K. Lam, No-switching quantum key distribution using broadband modulated coherent light, *Phys. Rev. Lett.* **95**, 180503 (2005).

[50] C. M. Caves and P. D. Drummond, Quantum limits on bosonic communication rates, *Rev. Mod. Phys.* **66**, 481 (1994).

[51] U. Leonhardt, *Measuring the quantum state of light*, Vol. 22 (Cambridge university press, 1997).

[52] M. Dall’Arno, G. M. D’Ariano, and M. F. Sacchi, Purification of noisy quantum measurements, *Phys. Rev. A* **82**, 042315 (2010).

[53] I. Devetak and A. Winter, Distillation of secret key and entanglement from quantum states, *Proc. R. Soc. A* **461**, 207 (2005).

[54] P. J. Coles, E. M. Metodiev, and N. Lütkenhaus, Numerical approach for unstructured quantum key distribution, *Nat. Commun.* **7**, 11712 (2016).

[55] A. Winick, N. Lütkenhaus, and P. J. Coles, Reliable numerical key rates for quantum key distribution, *Quantum* **2**, 77 (2018).

[56] P. Dong, L. Chen, C. Xie, L. L. Buhl, and Y.-K. Chen, 50-gb/s silicon quadrature phase-shift keying modulator, *Opt. Express* **20**, 21181 (2012).

[57] Y. Zhang, Z. Chen, S. Pirandola, X. Wang, C. Zhou, B. Chu, Y. Zhao, B. Xu, S. Yu, and H. Guo, Long-distance continuous-variable quantum key distribution over 202.81 km fiber, *Phys. Rev. Lett.* **125**, 010502 (2020).

[58] T. Upadhyaya, T. van Himbeeck, J. Lin, and N. Lütkenhaus, Dimension reduction in quantum key distribution for continuous- and discrete-variable protocols (2021), arXiv:2101.05799.

[59] R. Renner, Security of quantum key distribution, *Int. J. Quantum Inf.* **6**, 1 (2008).